NASA

Technical Memorandum 84954

A Mechanism for Plasma Waves at the Harmonics of the Plasma Frequency in the Electron Foreshock Boundary

Alexander J. Klimas

DECEMBER 1982

National Aeronautics and Space Administration

Goddard Space Flight Center
Greenbelt, Maryland 20771

A MECHANISM FOR PLASMA WAVES AT THE HARMONICS OF THE PLASMA FREQUENCY IN THE ELECTRON FORESHOCK BOUNDARY

by

Alexander J. Klimas
NASA/Goddard Space Flight Center
Laboratory for Extraterrestrial Physics
Greenbelt, MD 20771

SUBMITTED TO: Journal of Geophysical Research

Abstract

A bump-on-tail unstable reduced velocity distribution has been constructed from data obtained at the upstream boundary of the electron foreshock by the GSFC electron spectrometer experiment on the ISEE-1 satellite. This distribution is used as the initial plasma state for a numerical integration of the 1-D Vlasov-Maxwell system of equations. The integration is carried through the growth of the instability, beyond its saturation, and well into the stablized plasma regime. A power spectrum for the electric field of the stabilized plasma is computed. The spectrum is dominated by a narrow peak at the Bohm-Gross frequency of the unstable field mode but it also contains significant power at the harmonics of the Bohm-Gross frequency. The harmonic power is in sharp peaks which are split into closely spaced doublets. The fundamental peak at the Bohm-Gross frequency is also split, in this case into a clcsely spaced triplet. The splitting is due to slow modulations of the stabilized electric field oscillations which, it is thought, are caused by wave-particle trapping. The wave length of the m'th harmonic of the Bohm-Gross frequency is given by λ_u/m where λ_u is the wave length of the unstable mode. The mechanism for excitation of the second harmonic is shown to be second order wave-wave coupling which takes place during that period in the evolution of the instability which would otherwise be called the linear-growth phase. It is conjectured that the higher harmonics are excited by the same mechanism. It is further argued that harmonic excitation at the boundary of the electron foreshock shculd be a common occurrence.

I. Introduction

The theory for the generation of electrostatic plasma waves near the electron plasma frequency upstream of the Earth's bow shock, as presented by Scarf et al. (1971), Fredricks et al. (1971) and by Filbert and Kellogg (1979), has been generally accepted. This acceptance developed regardless of the fact that the unstable electron velocity distributions predicted by the theory had never been observed (Feldman et al., 1973). Recently, observations made on the ISEE spacecraft (Anderson et al., 1981) have confirmed the presence of the necessary unstable distributions in the electron foreshock at times when significant electrostatic plasma waves were being detected. A further observation of an unstable velocity distribution in the electron foreshock is presented here; it was obtained by the GSFC electron spectrometer on the ISEE-1 spacecraft (Ogilvie et al., 1978). Simultaneous measurements of the electrostatic wave intensity obtained by the ISEE plasma wave investigation (Gurnett et al., 1978) and the ISEE electron density experiment (Harvey et al., 1978) are also presented. These measurements indicate that the unstable distribution was observed just as the spacecraft was passing through the upstream boundary of the electron foreshock.

The ISEE electron and plasma wave observations both motivate and enable a more detailed study of the unstable plasma evolution in the electron foreshock. The results of such a study are presented here.

A numerical code developed by Klimas (1982) has been used to integrate the Vlasov-Maxwell equations for a one-dimensional electron plasma forward in time from an assumed initial plasma state. The unstable velocity distribution observed by the GSFC electron spectrometer was used for the initial velocity distribution. The initial electric field was simply "seeded" with very low amplitude wave modes. The results which are presented show the evolution of the plasma from its initial "bump-on-tail" unstable state through saturation of the instability and considerably beyond.

An unexpected feature of the electric field evolution has been discovered. It was expected that the saturated electric field would simply oscillate at the Bohm-Gross frequency (essentially the electron plasma frequency) provided by the linearized electrostatic plasma dispersion equation (Bohm and Gross, 1949). It was found that not only the Bohm-Gross frequency but also all of its harmonics that could be included in the numerical code, given its present size, were excited to significant levels in the saturated field. The resulting power spectrum for the saturated electric field which is presented here shows a dominant peak at essentially the plasma frequency plus peaks near the $2f_p$, $3f_p$ and $4f_p$ positions which are further split into closely spaced doublets. The splitting is due to low frequency modulations of the harmonic field components presumably caused by wave-particle trapping effects. The peak at the plasma frequency is also split, in this case into three closely spaced peaks, but the central peak is so dominant that the other two are difficult to pick out.

An explanation of the harmonic excitation is given in section IV. A simple verbalization of that explanation is as follows: The initial plasma evolution is qualitatively as predicted by linearized plasma theory (Krall and Trivelpiece, 1973). Field modes whose phase velocities lie on parts of the initial electron velocity distribution with positive velocity and slope are unstable and grow exponentially with time. Other field modes Landau damp and therefore decay exponentially with time. All modes remain small, but the growing modes become very large compared to the decaying modes. At some point in the plasma evolution wave-particle coupling terms in the governing Vlasov equation which are quadratic in the growing modes become larger than other similar terms which are linear in the decaying modes. At that point the linearized description of the plasma fails and non-linear phenomena take over. Field modes which had earlier been decaying then are pumped by the dominant unstable mode which continues to grow. These pumped modes experience sudden shifts in their oscillation frequencies to harmonics of the unstable mode frequency. Interestingly, all of this occurs long before the saturation of the instability, during its "linear growth" phase when non-linear phenomena are not expected. By that time when the instability does saturate the pumped modes have grown considerably and the field is left with significant power at the harmonic frequencies.

The plasma model which is integrated numerically is a generalization of the usual Vlasov-Poisson system of equations obtained in the electrostatic limit. Maxwell's equation for the displacement current is added to the Vlasov (collisionless Boltzmann) and Poisson equations to provide a complete description of the plasma. The generalization and the motivation for it are discussed in detail in section II. Section III contains a discussion of various aspects of the numerical integration. First, the initial electron distribution obtained from the ISEE-1 electron spectrometer experiment is introduced. Through a comparison of electron heat flux measurements and simultaneous plasma wave observations it is argued that the bump-on-tail unstable initial distribution was obtained just as the ISEE-1 satellite was passing through the upstream boundary of the electron foreshock. Next some details of the calculated electric field are presented and finally the electric field power spectrum discussed above is presented. In section IV a calculation of the second harmonic excitation is given which is based on a linear plasma theory with second order wave-wave coupling included where necessary. A comparison of the results of this calculation with the numerical results indicates that the second harmonic excitation is due entirely to second order wave-wave coupling which takes place during the otherwise linear growth phase of the instability. It is conjectured that the higher harmonics are excited in a similar manner.

II. The Plasma Model

The results which are presented in this paper have been obtained using the following one-dimensional electron plasma model for the reduced electron distribution function, $F(x,v,\tau)$, and the electric field, $\mathcal{E}(x,\tau)$:

$$\frac{\partial F}{\partial \tau} + v\frac{\partial F}{\partial x} - \mathcal{E}\frac{\partial F}{\partial v} = 0 \qquad 1).$$

$$\frac{\partial \mathcal{E}}{\partial x} = 1 - \int_{-\infty}^{\infty} dv\ F \qquad 2).$$

$$\frac{\partial \mathcal{E}}{\partial \tau} = \int_{-\infty}^{\infty} dv \; v \; F \quad - \quad U \qquad 3).$$

These equations are dimensionless. In the following let the starred quantities be the original dimensional ones. Then $x = x^*/L$ where L is an arbitrary length scale. Solutions which are periodic in x^* over the interval $-L \leq x^* \leq L$ will be considered. Therefore 2L is the longest wavelength to be considered. Time is measured by $\tau = \omega_p t^* = 2\pi f_p t^*$ where f_p is the electron plasma frequency. Then $v = v^*/\omega_p L$ and $\mathcal{E} = \mathcal{E}^*/4\pi e n_o L$ where n_o is the electron density averaged over the interval of periodicity; it is a property of periodic solutions of equations 1-3 that n_o is a constant in τ. The longest time scale of interest is approximately 10 ms and the longest length scale is several tens to perhaps approximately 100 Debye lengths. Thus, the ion density is assumed constant and equal to n_o; the one in equation 2 stands for the dimensionless ion density. The magnetic field is also assumed constant in τ and only weakly dependent on position. The variable, x, measures position along the local magnetic field direction and the electric field is assumed linearly polarized in the magnetic field direction. The evidence that is available is consistent with the assumption that the electron plasma oscillations in the foreshock are indeed polarized along the local magnetic field (Anderson, et al., 1981). The weak spatial dependence of the magnetic field is ignored in equation 1; this is equivalent to ignoring the electron drifts. Equation 3 is derived from Maxwell's equation,

$$4\pi \vec{J} + \frac{\partial \vec{\mathcal{E}}}{\partial t} = c\left(\vec{\nabla} \times \vec{B}\right)$$

If $\vec{v} \times \vec{B}$ were exactly zero then U, in equation 3, would be the dimensionless ion velocity component along the magnetic field. Because of the factor, c, in this equation, however, even small values of $\vec{v} \times \vec{B}$ might be expected to contribute. Thus, in equation 3, U is the ion velocity component modified by the component of $c\,(\vec{v} \times \vec{B})$ along $\vec{B}$. In any case U is treated as a constant. The net result is a model for high frequency and small wavelength electron plasma phenomena superimposed on a neutralizing ion-magnetic field background which varies only very weakly on those small scales. Solutions are sought subject to initial data F(x,v,0) with

$$\int_{-\infty}^{\infty} dv \; F(x,v,0) = 1$$

and $\mathcal{E}_o(0)$ where $\mathcal{E}_o(\tau)$ is the spatial average (or zero'th Fourier mode) of the electric field.

It is perhaps more traditional when studying electron plasma phenomena to study the electrostatic limit governed by the Vlasov-Poisson system of equations, equations 1 and 2. But equations 1 and 2 do not determine $\mathcal{E}_o(\tau)$. Within the Vlasov-Poisson tradition $\mathcal{E}_o(\tau)$ is normally set to zero and ignored. It was felt that this assumption would be a poor one in the foreshock which is strongly influenced by the bow shock and hardly contains homogeneous plasma. It would certainly be a completely untenable assumption when, as intended, non-periodic solutions are considered. Thus, the additional equation 3 has been included to complete the description of the plasma, including its space-averaged electric field mode. Any solution of equations 1-3 is also a solution of the Vlasov-Poisson system, but, with its space-averaged electric field governed by another of Maxwell's equations. Equations 1-3 will be referred to as the Vlasov-Maxwell system of equations for a 1-D electron plasma.

Klimas and Cooper (1982) have shown that any periodic solution of the Vlasov-Maxwell system of equations of the type discussed above can be transformed into a similarly periodic solution of the Vlasov-Poisson system with $\mathcal{E}_o(\tau) = 0$ for all τ, and visa-versa. The numerical integration results which are presented in section III are for solutions of equations 1-3 which are appropriate, as discussed above, for the foreshock region. In section IV, however, where an analytical analysis of the numerical results is given, the Vlasov-Poisson system (equations 1 and 2 with $\mathcal{E}_o(\tau) = 0$) will be used in order to take advantage of the many techniques which have been developed for analysis of that system. Then the transformation of Klimas and Cooper will be used to transform the results of that analysis to predictions for the behavior of the numerical solutions.

III. Numerical Results

In this section a solution of equations 1-3 will be presented using an initial distribution, derived from data obtained by the ISEE-1 Electron Spectrometer Experiment, which is unstable to the bump-on-tail instability. The numerical integration method developed by Klimas (1982) has been used to obtain these results. This is a periodic solution which is presented here as only a first step in a program of research leading to non-periodic solutions which can include the influence of the nearby bow shock in a more cogent manner.

a). Electric Field

The numerical predictions for the electric field will be presented here in terms of $E(\tau) = (L/\lambda_p)\,\mathcal{E}(\tau)$. This scaling for the electric field leads to the following useful rule: When $E(\tau) = 1$, then the energy density in the electric field equals the total kinetic energy density in the initial state of the plasma. Since the kinetic energy of the plasma does not vary significantly it is true that when $E(\tau) = 1$ then the field and particle energy densities are essentially equal. In the foreshock, if this plasma state were reached then the electric field intensity would be roughly 1 V/m.

The output of the numerical integration scheme for the electric field can be writen,

$$E(x,\tau) = E_0(\tau) + \sum_{m=1}^{M}\left[A_m(\tau)\cos m\pi(x+U\tau+\phi) + B_m(\tau)\sin m\pi(x+U\tau+\phi)\right] \quad 4).$$

where

$$E_0(\tau) = \left(\frac{L}{\lambda_0}\right)\left[\mathcal{E}_0(0)\cos\tau + (u_0(0)-U)\sin\tau\right] \quad 5).$$

in which u_o is the space average of

$$u(x,\tau) = \int_{-\infty}^{\infty} dv \; v \; F$$

The quantity, $\phi(\tau)$, is given by,

$$\phi(\tau) = \int_{0}^{\tau} ds \; (\tau - s) \; \mathcal{E}_o(s) \qquad 6).$$

The quantity, $\mathcal{E}_o(0)$, is part of the initial data; it could be set to zero. If $F(x,v,0)$ is such that $u_o(0) - U = 0$, and if $\mathcal{E}_o(0)$ is set to zero, then $\mathcal{E}_o(\tau) = \phi(\tau) = 0$ and the expression for the electric field given by equation 4 reduces to the electrostatic limit. The solution presented here follows from an electron spectrometer observation for which $u_o(0) - U \neq 0$. Thus, the electrostatic limit cannot be reached for this solution even if it is assumed that $\mathcal{E}_o(0) = 0$. The $A_m(\tau)$ and $B_m(\tau)$ are obtained directly from the numerical calculation. These coefficients will be presented here; the total field can be reconstructed using equation 4. Only ‘ne field modes have been included in the solution which will be presented. Of course more modes are desirable and it is expected that more will be included in the future. On the other hand various solutions have been computed using varying numbers of modes and varying related phase velocities to ensure that the interpretation of the results which will be presented is not an artifact of the small number. It is not expected that an increased number of modes will lead to any significant change.

b). The Initial Data

The dots in Figure 1 represent a reduced distribution function which has been constructed from GSFC electron spectrometer data taken aboard the ISEE-1 spacecraft on November 6, 1977 at 11:38:13-16 UT. The construction of the reduced distribution function requires integration over the velocity components perpendicular to the local magnetic field. The spread in the dotted curves, where it occurs, is due to the difference in

integration results using two methods of integration. In principle the integration should be carried to infinite perpendicular velocity but, of course, the electron spectrometer has a finite upper energy limit. The upper dotted curve was obtained by extrapolating the electron spectrometer data smoothly to zero for very large velocity and the lower curve by setting the electron distribution to zero for all high velocities where it was not measured; in each case the integration over the perpendicular velocity components was then carried out. From the results it appears that at least in this case, the reduced distribution is very well determined by the electron spectrometer data over the parallel velocity interval of significance to the evolution of plasma wave phenomena; i.e., the velocity interval containing the bump on the tail of the reduced velocity distribution.

The data in Figure 1 were apparently collected as the spacecraft was passing through the boundary of the electron foreshock into interplanetary space. Figure 2 shows the electron heat flux determined from the electron spectrometer data over a one-hour interval which contains the time of the observation in Figure 1. The upper panel shows the heat flux magnitude, the middle panel the component of the heat flux vector in the ϕ-direction measured in the ecliptic plane from the Earth-Sun direction, and the bottom panel the component in the θ-direction measured from the ecliptic plane. The horizontal dashed lines in the middle and bottom panels show the directions parallel or anti-parallel to the nominal Parker spiral magnetic field. The heavy horizontal line segments give one minute averaged magnetic field data from the ISEE data pool tapes. The heat flux vector can be seen to be either parallel or anti-parallel to the magnetic field with abrupt transitions between. Figure 3 shows electric field data obtained by the Iowa Plasma Wave Experiment aboard ISEE-1 during the same time interval. The electron plasma frequency lies in the 31.1 kHz channel during this time. Figures 2 and 3 together show the high correlation between intense plasma wave noise in the vicinity of the plasma frequency and reversals of the heat flux vector away from its normal interplanetary direction along the field and away from the sun. This correlation has been known for some time (Ogilvie et al., 1971; Scarf et al., 1971; Fredricks et al., 1971; Feldman et al., 1973) and is generally interpreted as entry into

the electron foreshock. The reduced distribution in Figure 1 was constructed from data obtained during the heat flux reversal which can be seen in Figure 2 at approximately 11:38. Probably because this short reversal occurs just at the edge of a gap in the plasma wave data, it is not clearly evident in that data. Figure 4 contains a more detailed spectrogram obtained by the ISEE-1 electron density experiment over a fifteen minute period starting at 11:30 and containing the time of the electron observation. The frequency scale of the spectrogram ranges from essentially 0 to 50 kHz and the grey scale indicated on the right of the figure is adjusted to cover from 16 to 72 dB above the 1 nV m^{-1} $Hz^{-1/2}$ level. The short black bar on the top of the figure indicates a time period during which the electron density sounder transmitter was on; this is the cause of the coincident data gap in Figure 3 in the plasma wave data. A scan of the heat flux data and the plasma wave data in Figures 2 and 3 shows that the satellite was in the electron foreshock at the start of the spectrogram. The general increase in the level of noise in the plasma wave experiment 31.1 kHz channel at about 11:34 is clearly evident in the spectrogram, and in all of Figures 2, 3 and 4 the exit from the foreshock between 11:42 and 11:43 is very clear. The short heat flux reversal which starts, according to the electron spectrometer data, during 11:38:13-16 is also clearly evident in the spectrogram. The spectrogram contains 128 frequency steps, each of 400 Hz bandwidth, which are swept in a time period of 16 seconds starting at the lowest frequency and ending at the highest. The arrows labeled start and stop indicate the positions in two consecutive frequency sweeps at which the electron spectrometer observation of the unstable velocity distribution began and ended. About six seconds before the electron spectrometer observation the satellite was clearly imbedded in the foreshock. About six seconds after the electron spectrometer observation the spectrogram indicates a quiet field except for an intense peak at the plasma frequency. Presumably, due to velocity dispersion in the foreshock boundary, by the time at which this intense peak is observed the satellite has passed out of the foreshock as defined by the low energy electrons detectable by the electron spectrometer but it remains in the foreshock boundary defined by the beam of higher energy electrons arriving from the bow shock. This beam of higher energy particles continues to excite plasma noise at the plasma frequency. Thus,

it is concluded that the ISEE-1 satellite passed out of the foreshock shortly after 11:38, as the data for Figure 1 were being collected, and soon after passed back into the foreshock. It is assumed that this passage is not clear in the plasma wave experiment data because of the data gap.

The unstable bump-on-tail reduced distribution shown in Figure 1 is an example of a phenomenon which has been presumed to exist at the boundary of the foreshock for quite some time (Filbert and Kellogg, 1979). The electron spectrometer onboard the ISEE-1 spacecraft is the first experiment with high enough time and velocity resolution to yield that result. A search through the electron spectrometer data for other such examples is in progress; detailed results will be presented later. Time alising during the electron spectrometer three second data collection interval is still a possibility. However, at this point it appears that many of the foreshock boundary crossings have been resolved by the electron spectrometer and have been found to coincide with bump-on-tail unstable reduced distributions.

The solid curve in Figure 1 is a three Gaussian fit to the electron spectrometer data which has been used as the initial velocity distribution for the numerical solution to follow. This initial data contains a cold, dense core, a high temperature halo, and a beam of approximately 150 eV electrons moving away from the bow shock along the local magnetic field. The electric field was assumed to initially contain very low amplitude waves with phase velocities at the positions of the thin vertical lines in Figure 1. The wavelengths of the modes ranges from approximately 10 down to 2.5 Debye lengths (approximately 70 down to 18 meters). The modes with the largest phase velocity magnitudes are those with the longest wavelengths and the modes with phase velocities nearest the origin in velocity in Figure 1 are the ones with the shortest wavelength. Other solutions have been computed containing longer wavelength modes (Klimas, 1982), whose phase velocities were outside the position of the beam velocity. Those modes were found to simply damp away with increasing time and to play no role in the evolution of the instability. From linear plasma theory, field modes with phase velocity at the position of the far right vertical line, on the rising portion of the bump, are expected to be unstable and to, therefore, grow exponentially with time until the

instability saturates due to non-linear phenomena. All other modes are expected to decay exponentially with time (to Landau damp). The actual evolution of the field modes turned out to be considerably more complex.

c). The Solution

Figures 5a-d contain plots of the absolute values of $B_1(\tau)$ through $B_4(\tau)$ over more than one hundred plasma periods (approximately 3 ms. total elapsed time) starting at the initial plasma state. The A-coefficients differ from the B-coefficients only in details and therefore space will not be taken to present plots of them. A close examination of these figures will reveal that the curves are made up of a sequence of peaks of slowly varying amplitude. Each pair of peaks represents a single period of harmonic oscillation on this semi-log plot of the absolute values. Figure 5a, for $B_1(\tau)$, shows a classic example of instability growth and saturation. Following an initial transient the amplitude of $B_1(\tau)$ grows exponentially at a rate which can be predicted very accurately using a dispersion relation from linear plasma theory. The oscillation frequency of this mode is also very accurately predicted by the Bohm-Gross relation from linear plasma theory. (These issues will be discussed in detail in the next section.) The instability saturates at $\tau \approx 200$ leaving this mode oscillating at the Bohm-Gross frequency, very close to the plasma frequency, with slow modulations of the amplitude which are due presumably to particle trapping effects.

A detailed description of the computed electric field will be given in the following subsection. At this point, however, a brief argument can be given which shows that the dominant feature of the electric field is in good agreement with the field detected by the plasma wave experiment: The total field, following saturation, is dominated in the vicinity of the plasma frequency by the contributions of $B_1(\tau)$ and $A_1(\tau)$. From this numerical solution it would be expected that plasma wave noise near the plasma frequency with amplitude $\approx$ 100 mV/m and wavelength close to 70 meters should be detected by the plasma wave experiment. The calibration of the plasma wave experiment is such that the plot of the 31.1 kHz channel in Figure 3, which contains the plasma frequency, should reach full scale

at several tens of millivolts/meter (private communication, D. A. Gurnett, P.I., Plasma Wave Experiment). An examination of Figure 3 reveals that the period just preceding and following the time of the electron spectrometer observation is characterized by unusually strong plasma wave activity near the plasma frequency. The 31.1 kHz channel appears full scale or near full scale almost continuously. The 70 meter wavelength predicted by the numerical solution is smaller by about a factor of three than the 215 meter antenna used to obtain the data in Figure 3. Thus, the plasma wave experiment would be expected to detect an electric field oscillating near the plasma frequency with amplitude roughly 30 mV/m, just about its full scale field level and in agreement with the data presented in Figure 3.

The plot of $B_2(\tau)$ in Figure 5b provides the first evidence of quite unexpected evolution for this bump-on-tail instability. Initially $B_2(\tau)$ decays exponentially in time as expected with rate close to the Landau damping rate predicted by linear plasma theory. The reversal of this decay at $\tau \approx 70$, the subsequent exponential growth, and the simultaneous shift to a higher oscillation frequency were not expected. After all, none of the usual assumptions which one makes to justify the accuracy of the linear plasma theory appear violated during this reversal but it is clear that the linear plasma theory (or even quasi-linear theory (Davidson, 1972)) would not allow such behavior. This situation is made even more difficult by the plots of $B_3(\tau)$ and $B_4(\tau)$ in Figures 5c and 5d which show more dramatic examples of the same kind of behavior. It would appear that the number of modes involved in this behavior is limited here by the number of modes included in the calculation and not by any feature of the physical phenomenon involved. On the other hand it is important to realize that not all possible field modes are involved. Other numerical solutions have been computed containing electric field modes with wavelengths longer than that of the unstable mode in this run; those field modes did not experience a reversal of their Landau damping. In addition, it has been found that field modes with wavelengths shorter than the unstable mode which, however, do not satisfy $\lambda_m = \lambda_u/m$, where λ_u is the unstable mode wavelength and m is any integer greater than one, also do not take part in the decay reversal and frequency shift. The solution presented here has been arranged so that the unstable mode is at the longest wavelength, all other modes are at

shorter wavelengths, and they all satisfy $\lambda_m = \lambda_u/m$. Thus, in this solution, only those modes that can reverse have been included because, in addition to the unstable mode, those are the only modes which rise to high enough amplitudes to make measurable contributions to the electric field.

d). The Electric Field Power Spectrum

The spectral distribution of the computed electric field is considerably richer than was expected. The electric field is not limited to plasma oscillations at (or very near) the plasma frequency. The decay reversals and simultaneous shifts to higher frequencies discussed above lead to a power spectrum with peaks at all the harmonics (limited only by the numer of modes in the numerical calculation) of the fundamental Bohm-Gross frequency. In addition these peaks are split into doublets or triplets due to the amplitude modulations evident in Figures 5a-d following saturation of the plasma instability at $\tau \approx 200$.

Figure 6 contains the electric field power spectrum computed from the output of the numerical calculation and, also, a power spectrum of a model electric field which is used to help interpret the numerical results. The electric field was computed using equation 4 with U = 0; this is the field in the reference frame moving with the solar wind. It will be shown below that the wavelengths in the electric field are quite small. As a result, the Doppler shifts associated with the transformation from solar wind to satellite frame of reference turn out to be very small corrections to the frequencies of the important field modes and, in general, can be ignored. The constant, $\mathcal{E}_o(0)$, nas been set to zero in order to present the simplest case. The vertical tick marks at the top of the figure give the positions of the plasma frequency and two, three and four times the plasma frequency. The spectrum was computed from that portion of the solution following the saturation of the instability, from $\tau \approx 200$ to $\tau \approx 630$. The field prior to $t \approx 200$ is relatively much weaker and after 200 shows no evidence for further qualitative evolution. Thus, it is felt that this portion of the solution yields the electric field that the plasma wave experiment should detect when it detects peaks in the electric field at the foreshock boundary. The heavy curve gives the power spectrum computed from the

numerical solution. Because the time interval over which the electric field was computed is short there is considerable leakage in this spectrum. To evaluate this effect a power spectrum for a model of the numerical field was also computed. A model electric field with pure harmonics at the Bohm-Gross frequency of the unstable mode and at two, three and four times that frequency was constructed. The amplitudes of each of the harmonics were chosen using the following reasoning: It was found that each of the well separated groups of peaks in the power spectrum came from distinct wavelengths in the field. The peaks in the vicinity of the Bohm-Gross frequency corresponded to the longest wavelength, or the $m = 1$ terms in equation 4. The peaks in the vicinity of twice the Bohm-Gross frequency come from the next shorter wavelength, half the longest, or the $m = 2$ terms in equation 4. And so on. The following general rule seems to apply. After the decay reversal and frequency shift at $\tau = 70$, each of the field modes that satisfy $\lambda_m = \lambda_u/m$ experiences a shift in oscillation frequency such that its phase velocity, ω_m/λ_m, moves up to that of the unstable mode; i.e., up to the rising portion of the bump on the reduced velocity distribution. All of these modes then have the same phase velocity and their oscillation frequencies are given by $\omega_m = m\,\omega_u$ where ω_u is the Bohm-Gross frequency of the unstable mode. None of these modes with $m > 1$ satisfy a dispersion relation; they are not normal modes of the plasma. Because each group of peaks in the power spectrum had its source in a single m-value in the sum of equation 4 it became a relatively simple matter to choose the amplitudes of the harmonics in the model electric field. The electric field contributions of each of the m-values in the sum were scanned for a maximum value. These maxima were then used for the amplitudes of their respective (same m-value) pure harmonics. The power spectrum of this model field made up of pure harmonic oscillations was then computed; the thin curve in Figure 6 is the result. The overall shift upward from the heavy to the thin curve is due to the choice of the maxima for the amplitudes of the pure harmonics. It is clear from the model field spectrum that there is indeed considerable leakage. The true spectrum for the model field, if it were computed over an infinite time interval, would consist of spikes at the Bohm-Gross frequency and its harmonics with no power in between. It is also clear from Figure 6 that the computed field power spectrum is consistent with power in isolated peaks each of which are

split into several closely spaced components. The second, third and fourth harmonics are clearly split into doublets and the first harmonic appears to be split into a triplet. This splitting of the peaks in the power spectrum is due to the slow amplitude modulations evident in Figures 4a-d after τ = 200 which are due probably to particle trapping in the electric field.

IV. A Mechanism for Higher Harmonic Excitation

It is thought that the decay reversals and frequency shifts discussed in the previous section can be explained in terms of a second order wave-wave coupling mechanism. This mechanism allows the unstable plasma mode to pump the stable ones to significant amplitudes with oscillation frequencies that are narmonics of the unstable mode frequency. A specific calculation of the amplitude, growth rate, and oscillation frequency of the second harmonic is given in this section. The results of this calculation are in excellent agreement with the numerical computation. It is conjectured that the higher harmonics are due to the same mechanism involving many more wave-wave couplings but a detailed calculation of the higher harmonics has not been done.

The calculation of the second harmonic excitation is essentially a linear calculation with second order coupling added where appropriate. As discussed above, the calculation will be done in the electrostatic limit (i.e., solutions of equations 1 and 2 with the constraint $\mathcal{E}_0(\tau) = 0$ will be studied) and the results will then be transformed to allow a comparison with the numerical computation. Therefore, consider solutions of equations 1 and 2 with $\mathcal{E}_0(\tau) = 0$ which are periodic in x over the interval $-1 \leq x \leq 1$ and are subject to initial data F(x,v,0). As in the numerical computation, let $F(x,v,\tau)$ and $\mathcal{E}(x,\tau)$ be represented by truncated Fourier series expansions in x with coefficients given by

$$f_m(v,\tau) = \frac{1}{2}\int_{-1}^{1} dx\ e^{-im\pi x} F(x,v,\tau)$$

and

$$\mathcal{E}_m(\tau) = \frac{1}{2}\int_{-1}^{1} dx\ e^{-im\pi x}\, \mathcal{E}(x,\tau)$$

Then, these coefficients satisfy

$$\frac{\partial f_m}{\partial \tau} + im\pi v f_m = \sum_{n=-M}^{M} \epsilon_{m-n} \frac{\partial f_n}{\partial v} \qquad 7).$$

$$\epsilon_m = \frac{i}{m\pi} \int_{-\infty}^{\infty} dv \; f_m \qquad (m \neq 0) \qquad 8).$$

and $\epsilon_o = 0$. Due to the truncation equations 7 and 8 govern those coefficients which satisfy $|m| \leq M$ and in the summation in equation 7 $|m-n| \leq M$ and $|n| \leq M$ where M is some integer greater than zero. In the numerical results presented in the previous section and for the rest of this calculation $M = 4$. All other coefficients are assumed zero.

To proceed assume that the plasma contains only very weak plasma waves, i.e., assume that $f_m << f_o$ for $m \neq 0$ and assume further that the f_m are well behaved as $|v| \to \infty$ such that the ϵ_m calculated from equation 8 are similarly small. These are standard assumptions which one would make in order to proceed with a linear theoretical treatment of equations 7 and 8. This will be the approach taken here until an obvious contradiction to the linear theory is found. Since $\epsilon_{-m} = \epsilon_m^*$ only $m \geq 0$ will be considered. Thus, consider the linear approximation to equations 7 and 8 starting with $m = 0$.

a). $m = 0$

$$\frac{\partial f_o}{\partial \tau} = 0 \qquad 9).$$

There are no linear terms in the summation of equation 7 because $\epsilon_o = 0$. Thus, $f_o(v,\tau) = f_o(v,0) \equiv g(v)$.

b). $m = 1$

This is one of the unstable modes. The linear approximation to equation 7 is

$$\frac{\partial f_1}{\partial \tau} + i\pi v f_1 = \epsilon_1 g \qquad 10).$$

Of course the problem of finding a solution to equations 8 and 10 for f_1 and ϵ_1 is a familiar one; the approach taken here is due originally to Landau (1946). Let $\tilde{f}_1(v,p)$ and $\tilde{\epsilon}_1(p)$ be the Laplace transforms of f_1 and ϵ_1 with the symbol, p, for the Laplace variable. Then,

$$\tilde{f}_1(v,p) = \frac{f_1(v,0)}{p + i\pi v} + \left(\frac{\tilde{\epsilon}_1(p)}{p + i\pi v}\right) g(v) \qquad 11).$$

and,

$$\tilde{\epsilon}_1(p) = \frac{i}{\pi D_1(p)} \int_{-\infty}^{\infty} dv \left(\frac{f_1(v,0)}{p + i\pi v}\right) \qquad 12).$$

where,

$$D_m(p) = 1 - \frac{i}{m\pi} \int_{-\infty}^{\infty} dv \left(\frac{g(v)}{p + im\pi v}\right) \qquad 13).$$

With $f_0(v,0)$ and $f_1(v,0)$ given by the sum of three gaussians in v, as in the case here, the method of Jackson (1960) can be used to find the zero in $D_1(p)$ which leads to the simple pole in $\tilde{\epsilon}_1(p)$ that dominates $\epsilon_1(\tau)$ as τ grows large. With,

$$\tilde{\epsilon}_1(p) = \frac{a}{p - p_o} \qquad 14).$$

where $p_o = \sigma + i\,\omega$, the result of this calculation is $\sigma = .0481$, a positive growth rate and therefore an unstable mode, and $\omega = -1.07$ (remember that in these dimensionless units $|\omega| = 1$ corresponds to oscillations at the plasma

frequency). Generally, the method of Jackson, when it applies, gives a more accurate result for ω than does the Bohm-Gross expression. However, in this particular case, with $m = 1$, the two results are essentially identical and therefore this frequency has been referred to everywhere else in this paper as the Bohm-Gross frequency of the unstable mode. The lowest frequency peak in the model field power spectrum (the thin curve) of Figure 6 is at this calculated Bohm-Gross frequency. The excellent agreement between the position of this peak and that derived from the numerically computed field (the heavy curve) indicates the accuracy with which the linear theory predicts the oscillation frequency of this unstable mode. Figure 7 shows the details of $B_1(\tau)$ during its linear growth phase. The slope of the solid line drawn on that figure can be used to calculate the actual growth rate of the instability; the result is .0530 as opposed to the calculated $\sigma = .0481$. Thus, the growth rate of the unstable mode is also very well predicted by the linear theory. Generally, the behavior of the unstable modes during their linear growth phase is very well predicted by the linear plasma theory.

c). $m = 2$

This is the first of the modes which experience the reversal of their Landau damping and the subsequent growth and frequency shift which are both in violation of the linear theory. It will be shown here that the evolution of this mode during its decay and subsequent growth is governed by

$$\frac{\partial f_2}{\partial \tau} + i 2\pi v f_2 = \epsilon_2 \frac{\partial f_0}{\partial v} + \epsilon_1 \frac{\partial f_1}{\partial v} \qquad 15).$$

At $\tau = 0$, f_2 and f_1 are equal in amplitude as are ϵ_2 and ϵ_1. All of these quantities are very small. Thus, the last term in this equation, which is quadratic in these small quantities, is initially completely negligible. With the neglect of this last term, both f_2 and ϵ_2 obey the same linear theory discussed above in the $m = 1$ case. A similar calculation of σ and ω in this case yields $\sigma = -.151$ and $\omega = -1.27$ in excellent agreement with the

behavior indicated in Figure 8 of $B_2(\tau)$ during its initial decay. However, the neglect of the last term in equation 15 cannot remain valid. While the linear theory applies $\mathcal{E}_1$ and f_1 are growing exponentially in time and $\mathcal{E}_2$ and f_2 are decaying exponentially in time. At some point the last term must dominate the right-hand side of this equation. In this subsection the effects of the last term, when it dominates, are calculated. It is shown that the decay reversal and frequency shift of $B_2(\tau)$ are thereby completely explained.

Using equations 15 and 8, it can be shown that the Laplace transform of $\mathcal{E}_2(\tau)$ is given by,

$$\tilde{\mathcal{E}}_2(p) = \frac{i}{2\pi D_2(p)} \int_{-\infty}^{\infty} dv \left(\frac{f_2(v,0)}{p + i2\pi v} \right)$$

$$+ \frac{i}{2\pi D_2(p)} \int_{-\infty}^{\infty} dv \, (p + i2\pi v)^{-1} \frac{1}{2\pi i} \int_C dp' \, \tilde{\mathcal{E}}_1(p') \, \tilde{f}'_1(v, p-p') \qquad (16).$$

in which $f'_1 = \partial f_1 / \partial v$ and the path of integration, C, is from $-i\infty$ to $+i\infty$ with $\tilde{\mathcal{E}}_1(p')$ analytic to the right and $\tilde{f}'_1(v, p-p')$ analytic to the left of the path on the complex p'-plane. The first term in this equation would be the sole result if a linear calculation were being done; it predicts the initial behavior of $B_2(\tau)$ while it is decaying. Let $\tilde{\mathcal{E}}_2(p) = \tilde{L}(p) + \tilde{Q}(p)$ where $\tilde{L}(p)$ is the linear first term in equation 16 and $\tilde{Q}(p)$ is the quadratic second term. With equation 14 for $\tilde{\mathcal{E}}_1(p)$,

$$\tilde{Q}(p) = \frac{i}{2\pi D_2(p)} \int_{-\infty}^{\infty} dv \left(\frac{a}{p + i2\pi v} \right) \tilde{f}'_1(v, p - p_o)$$

If equation 11 is used for f_1, then it can be shown that $\tilde{Q}(p)$ contains one term with a pole at $p = 2p_o$; this term is given by,

$$\tilde{Q}_2(p) = \frac{-a^2}{(p - 2p_o) D_2(p)} \int_{-\infty}^{\infty} dv \, \frac{g(v)}{(p + i2\pi v)^2 (p - p_o + i\pi v)}$$

Finally, the contribution of this pole to $\epsilon_2(\tau)$ is given by,

$$Q_2(\tau) = \left(\frac{a^2}{8\pi^2 D_2(2p_o)}\right) e^{2p_o\tau} \int_{-\infty}^{\infty} dv \left(\frac{\frac{\partial^3 f_o(v,o)}{\partial v^3}}{p_o + i\pi v}\right) \quad (17).$$

This expression gives a contribution to $B_2(\tau)$ which oscillates at exactly twice ω, the Bohm-Gross frequency of ϵ_1, and grows exponentially with twice the growth rate, σ, of B_1. The amplitude of this contribution to $B_2(\tau)$ is completely determined by the fit, in Figure 7, to the amplitude of $\epsilon_1(\tau)$ which yields $|a|$ and σ and by the calculation of ω done in the previous subsection; there are no free parameters available. The prediction from equation 17 for the amplitude of $B_2(\tau)$ is given by the straight line in Figure 8. The prediction from equation 17 for the oscillation frequency, 2ω, is given by the position of the second peak in the model field power spectrum in Figure 6 which lies just in the middle of the corresponding doublet determined from the numerical solution. It would appear that this contribution to $\epsilon_2(\tau)$ accounts entirely for the decay reversal and frequency shift to the second harmonic in $B_2(\tau)$ and thus, for the second harmonic excitation in the electric field. The mechanism for this contribution which has been examined above would normally be called second order wave-wave coupling but this is, perhaps, somewhat confusing terminology since it is actually the $m = 1$ mode interacting with itself which produces this result; it is hard to imagine a wave interacting with itself. Actually, the interaction is between the $m = 1$ wave in the electric field and the $m = 1$ density fluctuations in the particles; the terminology is simply inappropriate.

It is conjectured that the higher harmonics in the electric field are produced by the same mechanism as that which produces the second harmonic but, with more than just one mode doing the pumping. For example, after its decay reversal the third mode shifts to the third harmonic of the fundamental Bohm-Gross frequency and grows exponentially with a growth rate

which is three times that of the first mode. It is conjectured that this mode is governed by equation 8 and

$$\frac{\partial f_3}{\partial \tau} + i3\pi v f_3 = \epsilon_3 \frac{\partial f_0}{\partial v} + \epsilon_2 \frac{\partial f_1}{\partial v} + \epsilon_1 \frac{\partial f_2}{\partial v}$$

The first term on the right-hand side of this equation would provide the initial linear decay of $\epsilon_3(\tau)$ and the last two would do the pumping. As the index, m, increases the number of possible mode-mode couplings responsible for the pumping goes up rapidly.

V. Conclusion

The essential element which allowed the excitation of the harmonics in the example discussed in this paper was the large ratio of free energy in the electron beam to the field energy prior to the growth of the bump-on-tail instability. Thus, the unstable electric field modes grew by several orders of magnitude before the free energy was exhausted thereby leading to the important consequence that the linear growth phase of the instability lasted for a long time. During this long linear growth phase other shorter wavelength field modes which were Landau damping were able to decrease their strengths by several orders of magnitude. The result was a large imbalance between the strengths of the stable and unstable modes in the plasma; so large, in fact, that the linear Landau damping of the stable modes was eventually dominated by wave-wave coupling quadratic in the unstable modes. Although a quantitative statement cannot be made, it does seem safe to say that the thermal electric field noise level in the undisturbed interplanetary plasma at the frequencies and wavelengths of interest here is very small, probably smaller than the approximately 10^{-5} V/m which was used to seed the field modes in the numerical computation (Meyer-Vernet, 1979; Hoang et al., 1980; Couturier et al., 1981). Thus, the free energy of an electron beam at the foreshock boundary should easily dominate the undisturbed field energy. Certainly the plasma wave observations at the boundary of the foreshock are often consistent with a growth of several orders of magnitude in the field strength during the evolution of the instablity. It appears then that the excitation of harmonics at the boundary of the electron foreshock should be a common occurrence.

The numerical results which have been presented have been computed using only a small number of discrete field modes. However, various unreported numerical solutions have been computed to test the conclusions which have been given. It has been found that field modes with wavelengths longer than that of the unstable mode do not play any detectable role in the evolution of the unstable mode or the pumped modes. It has also been found that the same can be said of field modes with wavelengths shorter than that of the unstable mode whose wavelengths, however, do not satisfy the equation $\lambda_m = \lambda_u/m$. The solution which has been presented contains only field modes which do satisfy this equation with $1 \leq m \leq 4$. It is thought that only modes which satisfy this equation can possibly have a significant part in the evolution of the instability. Thus, it is thought that the solution which has been presented is essentially complete except for the modes which satisfy $\lambda_m = \lambda_u/m$ with $m > 4$. But the wavelengths of those modes, according to this equation, would be even shorter than the minimum 2.5 λ_D wavelength which is included here. It is not considered likely that field modes with wavelengths equal to λ_D or shorter would play a significant role if they were included but this point will be checked in the future when solutions with more field modes will be computed.

It is further not considered likely that the transition from the discrete modes appropriate for the numerical computation to a continuum of modes more appropriate for an interpretation of the plasma wave data would have any significant impact on the harmonic excitation. Following the long linear growth phase of the instability the contribution to the electric field from the continuum of unstable wavelengths should be dominated by those wavelengths which are very close to the most unstable wavelength. Because the field would therefore be dominated by a narrow range of wavelengths, and because the wavelength dependent Bohm-Gross correction to the plasma frequency is small, all of the important unstable field modes should oscillate at very nearly the same frequency, near the plasma frequency. With the resulting sharply peaked wavelength and frequency spectra for the unstable field modes it would be expected that the spectra for the pumped harmonic modes would be similarly peaked. Thus, it is expected that in the continuum, during the linear growth phase of the

instability and while the harmonic pumping is occurring, the field would evolve in a manner quite similar to that of the discrete mode calculation.

Then why have the harmonics of the plasma frequency not been observed at the electron foreshock boundary? The answer may be that they have been observed but due to the nature of the plasma wave detectors it is difficult to determine that this is the case. An unfortunate side effect of the high sensitivity of these detectors is their tendency to spill strong signals in any one frequency channel over into other nearby channels. A good example of this phenomenon can be seen in Figure 3 in which a very strong signal at the plasma frequency in the 31.1 kHz channel may be exciting many of the other frequency channels in the detector. There may also be harmonics of the plasma frequency in that data but that would be very difficult to prove. This is an extreme example; there may be other times when harmonics in the plasma waves could be separated from spillover in the detector. On the basis of the results of this paper it would appear that they are there to be found.

Acknowledgment

The author is grateful to the ISEE electron spectrometer, plasma wave, and electron density experimenters for providing their data and for engaging in many useful discussions. The ISEE Guest Investigator program provided partial support for the development of the numerical code used for integrating the plasma model. Special thanks to all of the members of the Information Analysis and Display Office at GSFC and to A. K. Tolbert for their help in developing the numerical code.

List of References

Anderson, R. R., G. K. Parks, T. E. Eastman, D. A. Gurnett, and L. A. Frank, Plasma waves associated with energetic particles streaming into the solar wind from the earth's bow shock, J. Geophys. Res., 86, 4493, 1981.

Bohm, D. and E. P. Gross, Theory of plasma oscillations. A. Origin of medium-like behavior, Phys. Rev., 75, 1851, 1949.

Couturier, P., S. Hoang, N. Meyer-Vernet, and J. L. Steinberg, Quasi-thermal noise in a stable plasma at rest: theory and observations from ISEE-3, J. Geophys. Res., 86, 11127, 1981

Davidson, R. C., Methods in Nonlinear Plasma Theory, p. 174, Academic Press, New York and London, 1972.

Feldman, W. C., J. R. Asbridge, S. J. Bame, and M. D. Montgomery, Solar wind heat transport in the vicinity of the earth's bow shock, J. Geophys. Res., 78, 3697, 1973.

Filbert, P. C., and P. J. Kellogg, Electrostatic noise at the plasma frequency beyond the earth's bow shock, J. Geophys. Res., 84, 1369, 1979.

Fredricks, R. W., F. L. Scarf, and L. A. Frank, Nonthermal electrons and high-frequency waves in the upstream solar wind, 2, Analysis and interpretation, J. Geophys. Res., 76, 6691, 1971.

Gurnett, D. A., F. L. Scarf, R. W. Fredricks, and E. J. Smith, the ISEE-1 and ISEE-2 plasma wave investigation, IEEE Trans. Geosci. Electr., GE-16, 225, 1978.

Harvey, C. C., J. Etcheto, Y. DeJavel, R. Manning, and M. Petit, The ISEE electron density experiment, IEEE Trans. Geosci. Electr., GE-16, 231, 1978.

Hoang, S., J. L. Steinberg, G. Epstein, and P. Tilloles, The low-frequency continuum as observed in the solar wind from ISEE-3: thermal electrostatic noise, J. Geophys. Res., 85, 3419, 1980.

Jackson, J. D., Longitudinal plasma oscillations, Plasma Phys., 1, 171, 1960.

Klimas, A. J., A numerical method based on the fourier-fourier transform approach for modeling 1-D electron plasma evolution, in press, J. Comp. Phys.

Klimas, A. J., and J. Cooper, The Vlasov-Maxwell and Vlasov-Poisson equations as models of a 1-D electron plasma, to appear in Phys. Fluids, 1983

Krall, N. A., and A. W. Trivelpiece, Principles of Plasma Physics, p. 458, McGraw-Hill Book Co., New York, 1973.

Landau, L. D., On the vibrations of the electronic plasma, J. Phys., U.S.S.R., 10, 25, 1946.

Meyer-Vernet, M., On natural noises detected by antennas in plasmas, J. Geophys. Res., 84, 5373, 1979.

Ogilvie, K. W., J. D. Scudder, and H. Doong, The electron spectrometer experiment on ISEE-1, IEEE Trans. Geosci. Electr., GE-16, 261, 1978.

Ogilvie, K. W., J. D. Scudder, and M. Sugiura, Electron energy flux in the solar wind, J. Geophys. Res., 76, 8165, 1971.

Scarf, F. L., R. W. Fredricks, L. A. Frank, and M. Neugebauer, Nonthermal electrons and high-frequency waves in the upstream solar wind, 1, Observations, J. Geophys. Res., 76, 5162, 1971.

List of Figure Captions

Figure 1 The dots indicate an electron reduced velocity distribution constructed from data obtained by the electron spectrometer experiment on ISEE-1 as it passed through the boundary of the electron foreshock. The solid curve is a three gaussian fit used for initial data for the numerical integration. The thin vertical lines indicate the initial phase velocities of the field modes included in the numerical integration.

Figure 2 Electron heat flux determined through a moment fit to data from the electron spectrometer experiment on ISEE-1 over a one hour interval which contains the time of the observation in Figure 1. The sudden shifts by approximately 180° in the angle ϕ indicate passage through the boundary of the electron foreshock.

Figure 3 Electric field measurements made by the plasma wave experiment on ISEE-1 using the 215 m. antenna over the same time interval contained in Figure 2. The plasma frequency during this time interval is in the 31.1 kHz channel. Sudden increases in the signal in this channel can be seen to be very well correlated with the heat flux reversals in Figure 2. The periodic data gaps occur when the electron density sounder experiment is turned on.

Figure 4 Electric field spectrogram made from data obtained by the electron density experiment on ISEE-1 over a fifteen minute time interval containing the time of the electron spectrometer observation in Figure 1. The spectrogram is constructed from consecutive 16 second frequency sweeps starting at the lowest frequency and ending at the highest. The beginning and end of the electron spectrometer observation are at the points indicated by the arrows labeled start and stop.

Figure 5 Four of the electric field modes obtained from the numerical integration of the 1-D Vlasov-Maxwell equations using the bump-on-tail unstable reduced velocity distribution given in Figure 1 for the initial plasma state. The mode labeled B_1 contains the unstable fundamental. The other three modes are initially stable but are later pumped by the unstable fundamental. The pumped modes oscillate at frequencies which are very close to the harmonics of the plasma frequency.

Figure 6 The heavy curve is a power spectrum constructed from the computed electric field following saturation of the bump-on-tail instability. The light curve is a power spectrum constructed in a similar manner from a model electric field containing power only at the Bohm-Gross frequency of the fundamental unstable mode and its harmonics; the power apparent in this curve between the peaks is due solely to leakage. A comparison indicates that the computed electric field contains power in isolated peaks, at the harmonics of the Bohm-Gross frequency, which are further split into closely spaced components.

Figure 7 The linear growth phase of the B_1 mode plotted in Figure 5a. The straight line is a fit which has been made to determine the magnitude of the oscillations in this mode and their growth rate. The growth rate determined in this manner is in very close agreement to the growth rate predicted by linear plasma theory.

Figure 8 The B_2 mode from Figure 5b during the linear growth phase of the bump-on-tail instability. The initial decay is as expected from linear plasma theory. The reversal of that decay and simultaneous frequency shift are due to pumping by the fundamental unstable mode through quadratic wave-wave coupling. The straight line is a no-free-parameter fit to the amplitude of this mode, during the pumping phase, calculated using the wave-wave coupling mechanism.

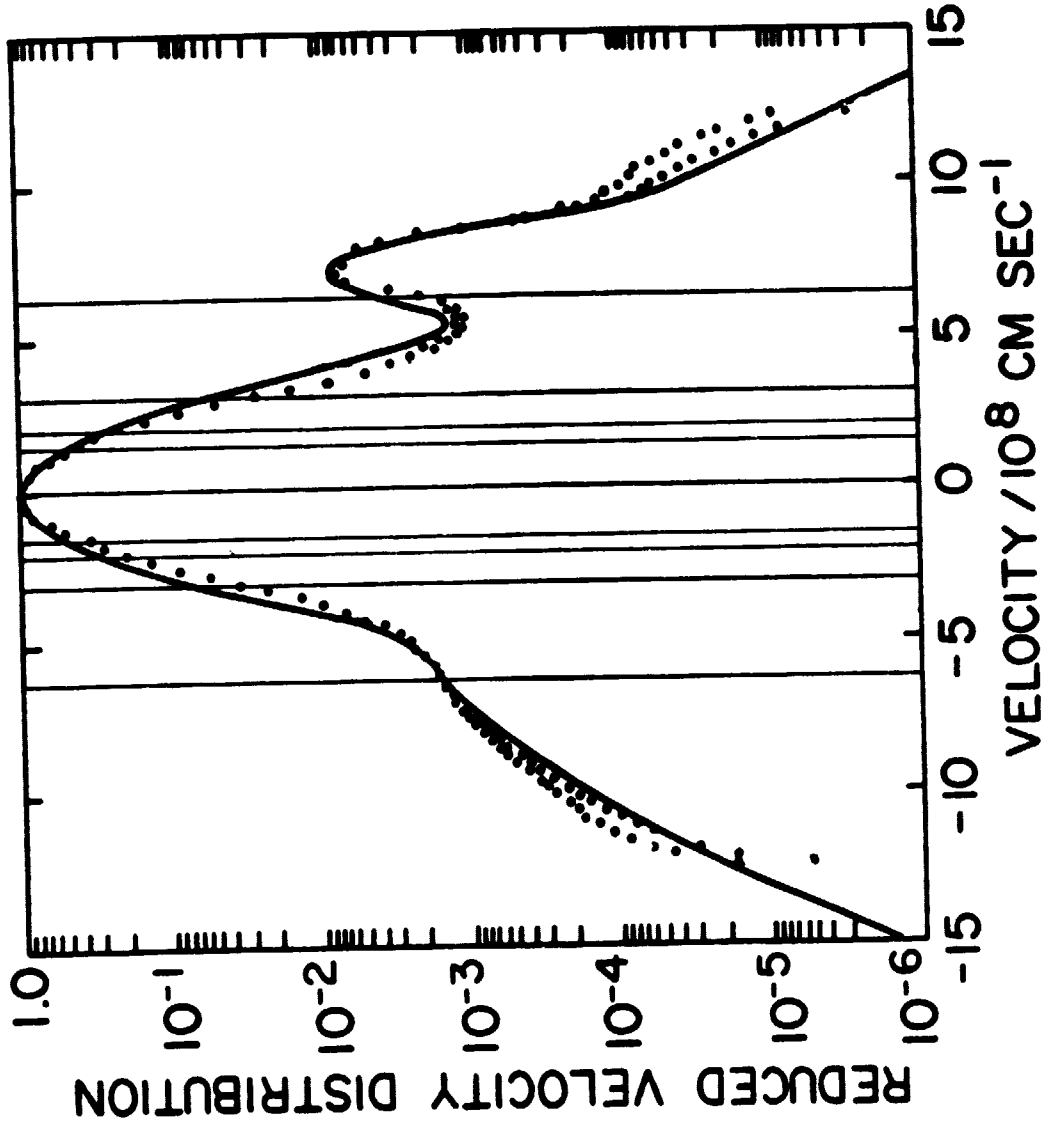

Figure 1

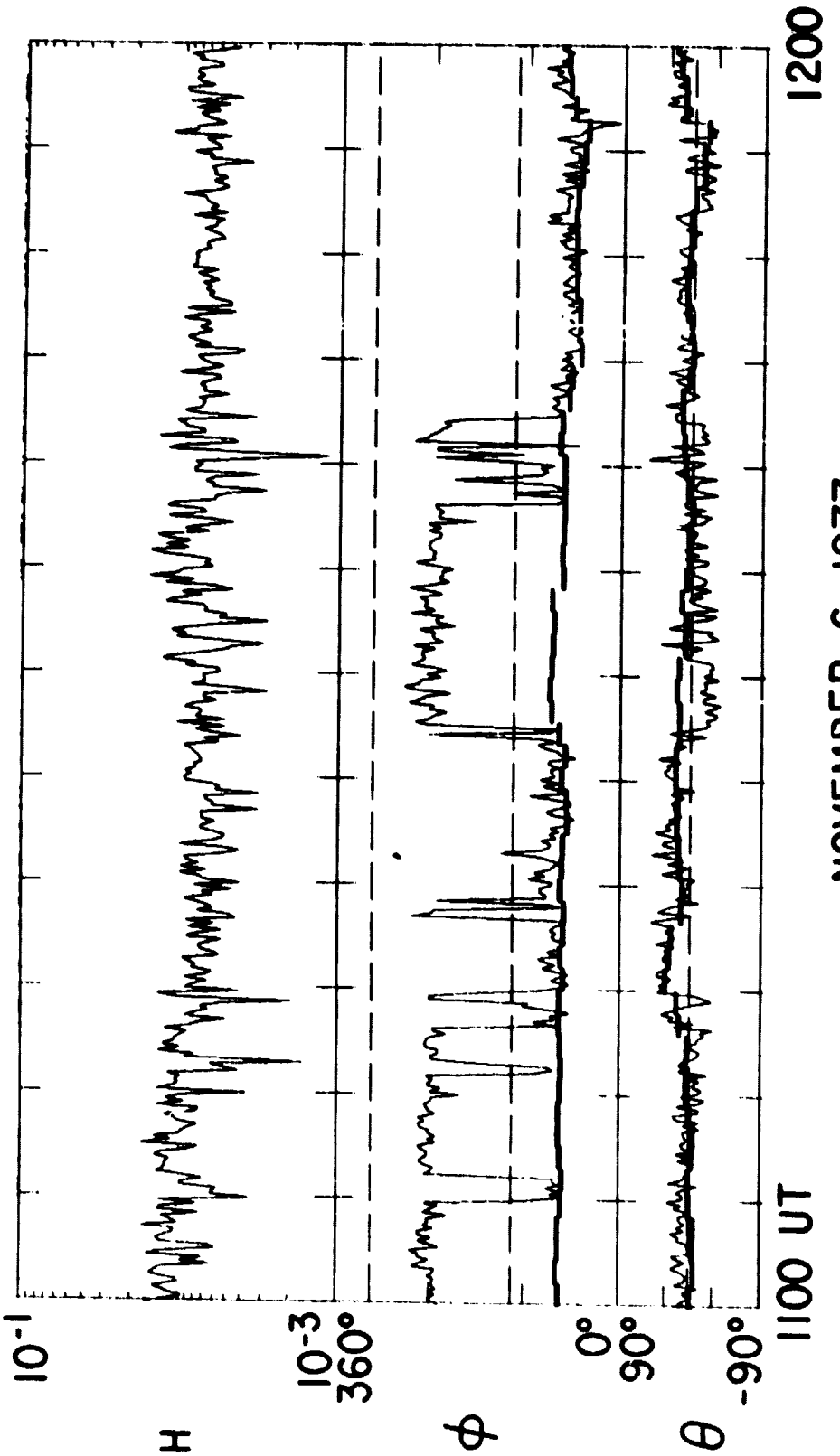

Figure 2

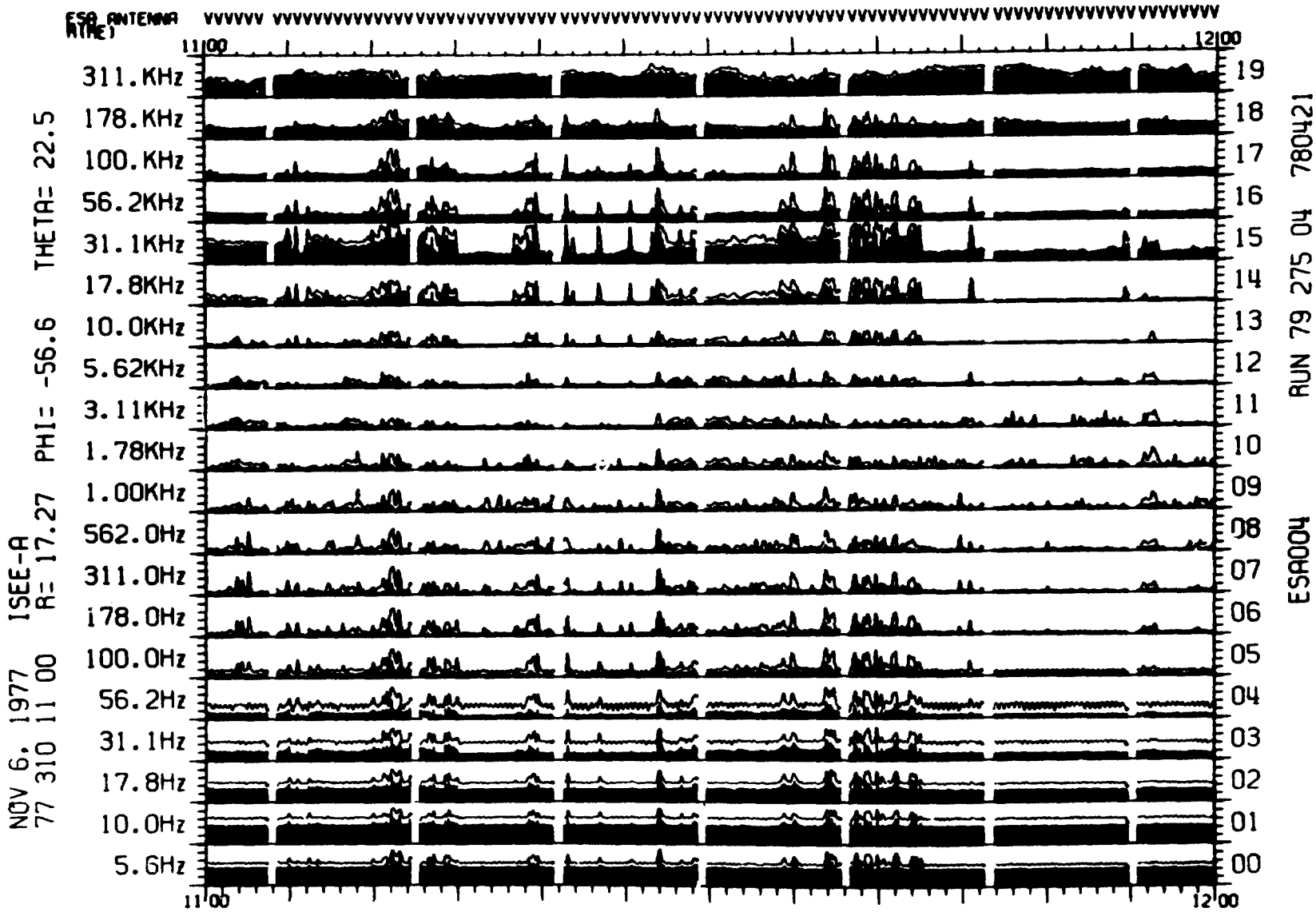

ORIGINAL PAGE IS
OF POOR QUALITY

Figure 3

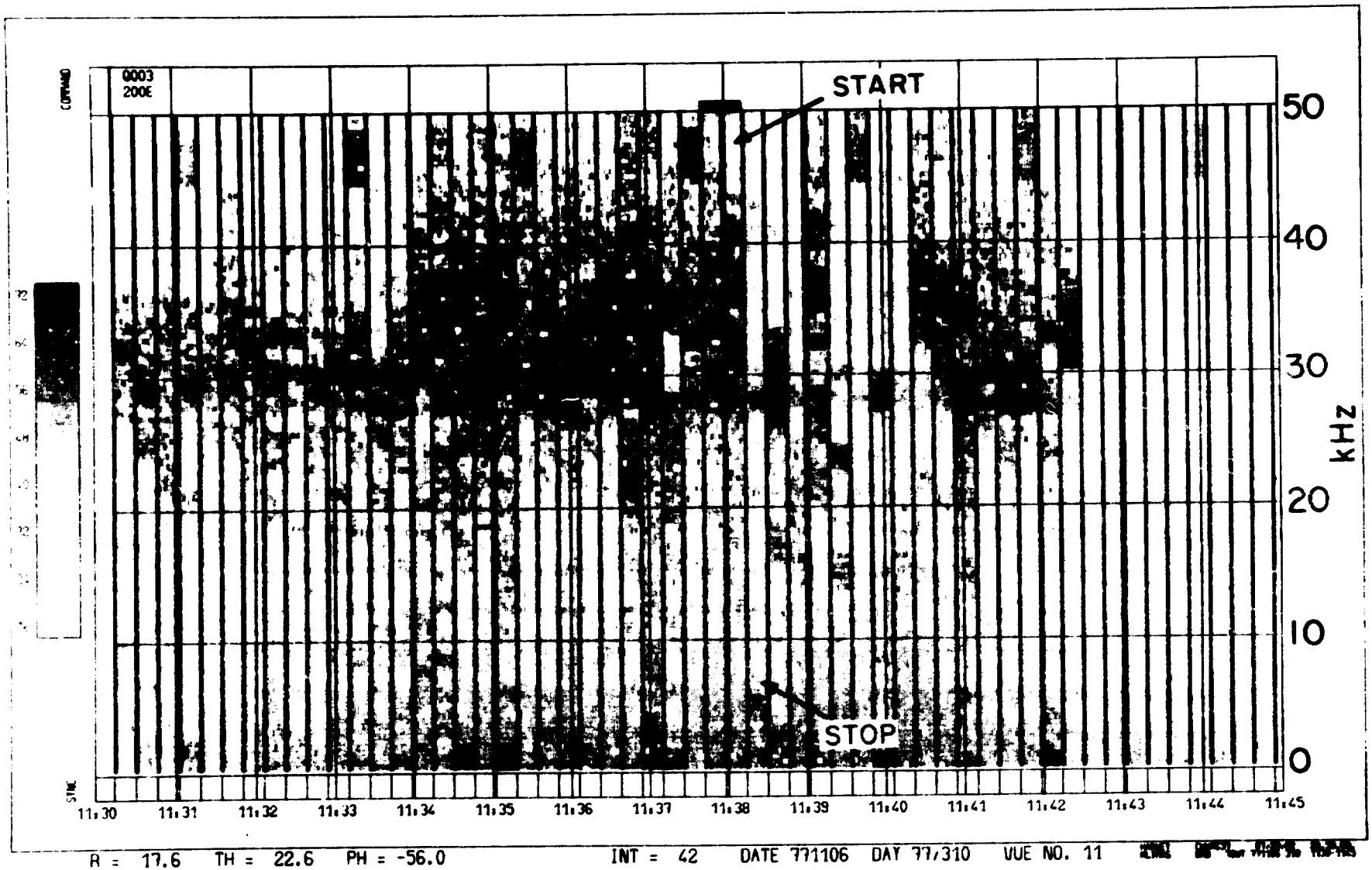

Figure 4

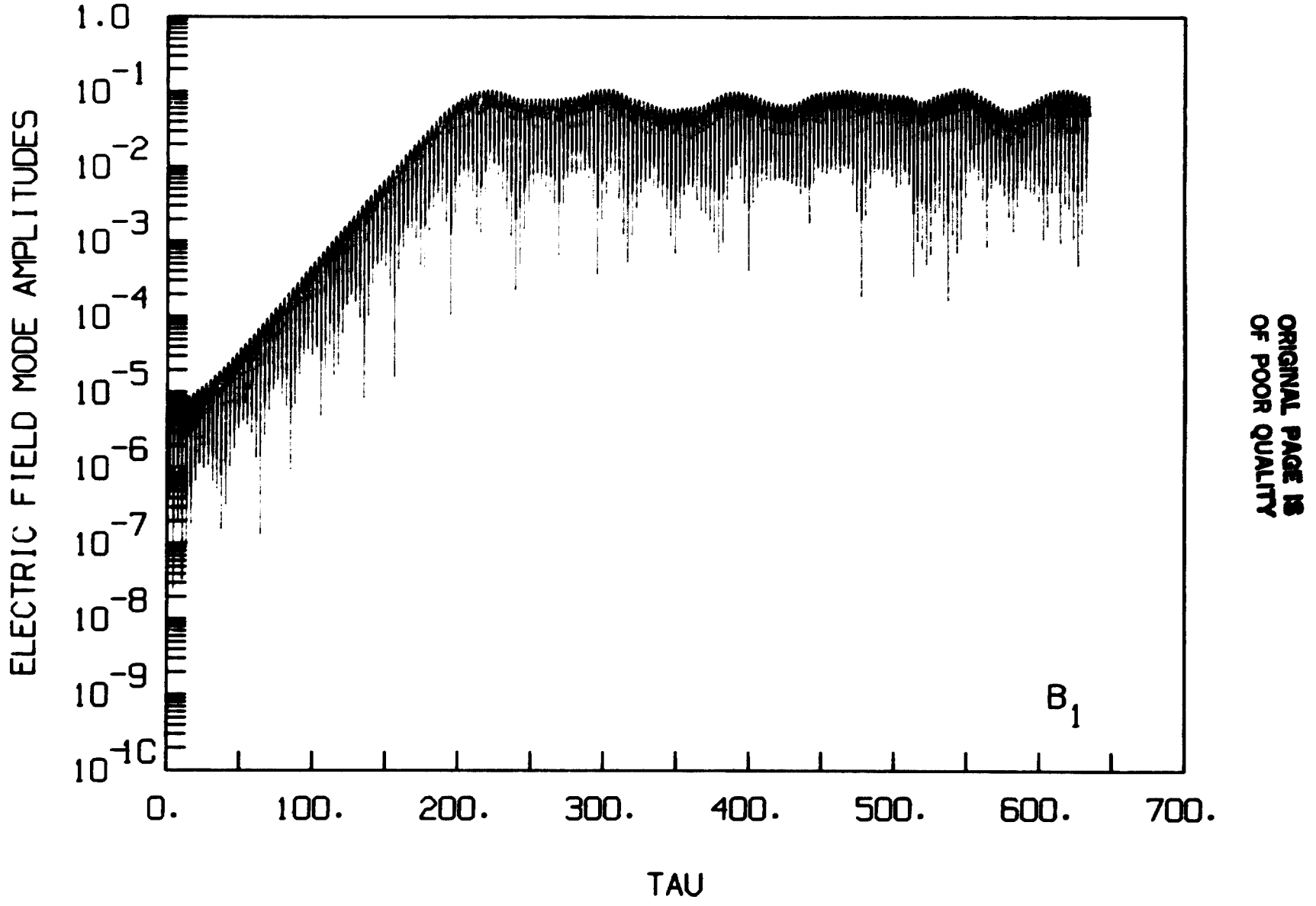

Figure 5a

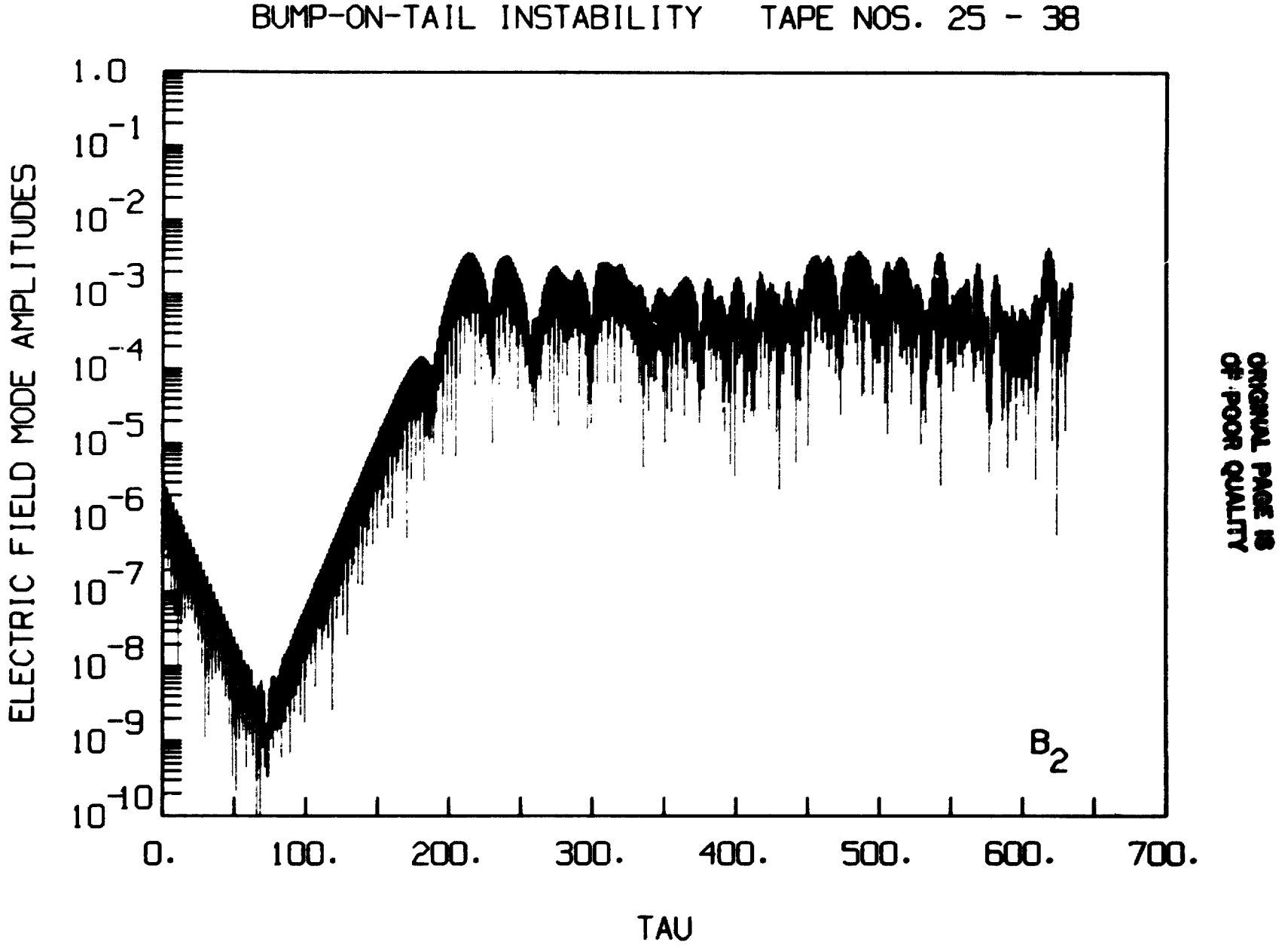

Figure 5b

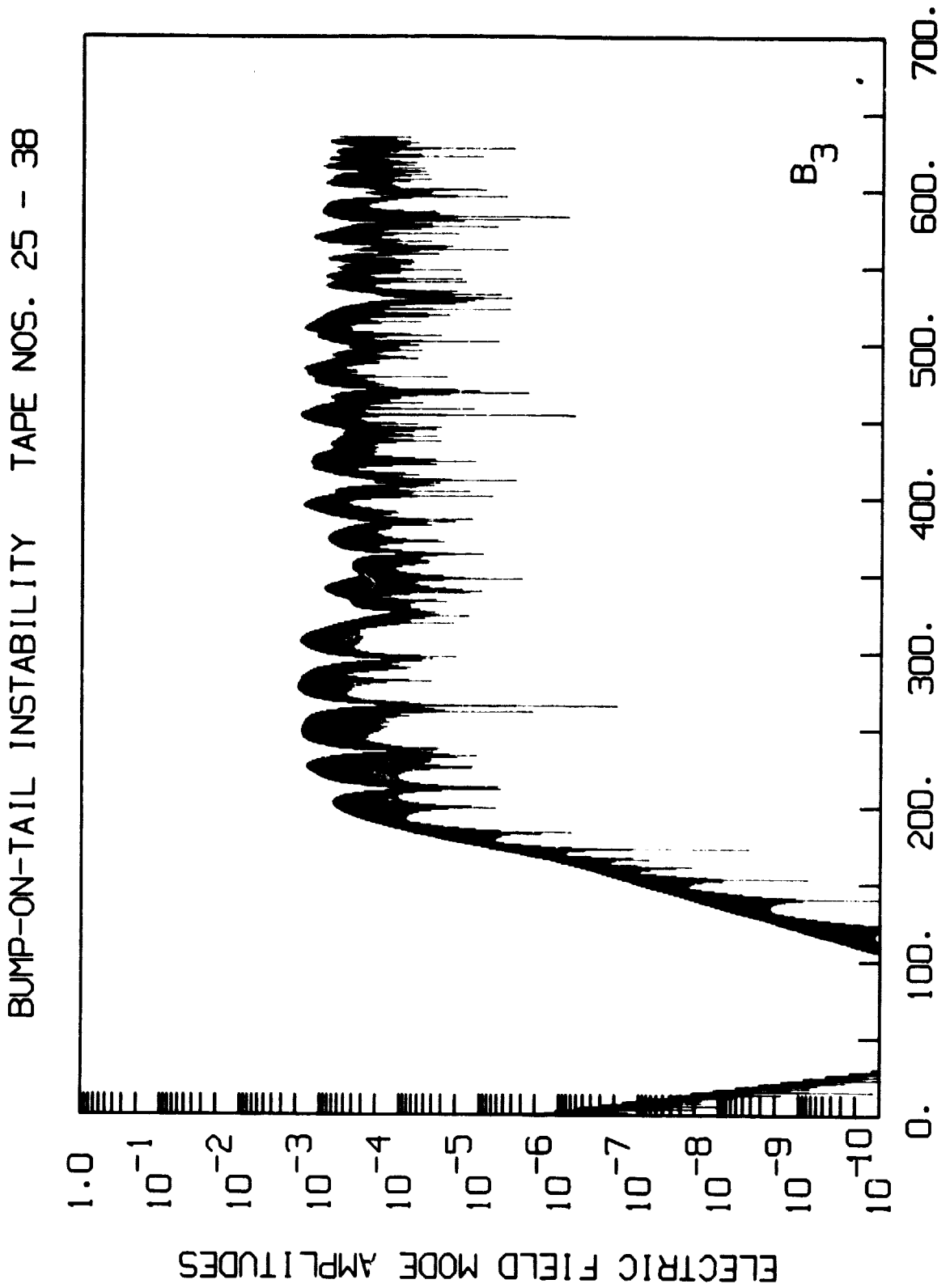

Figure 5c

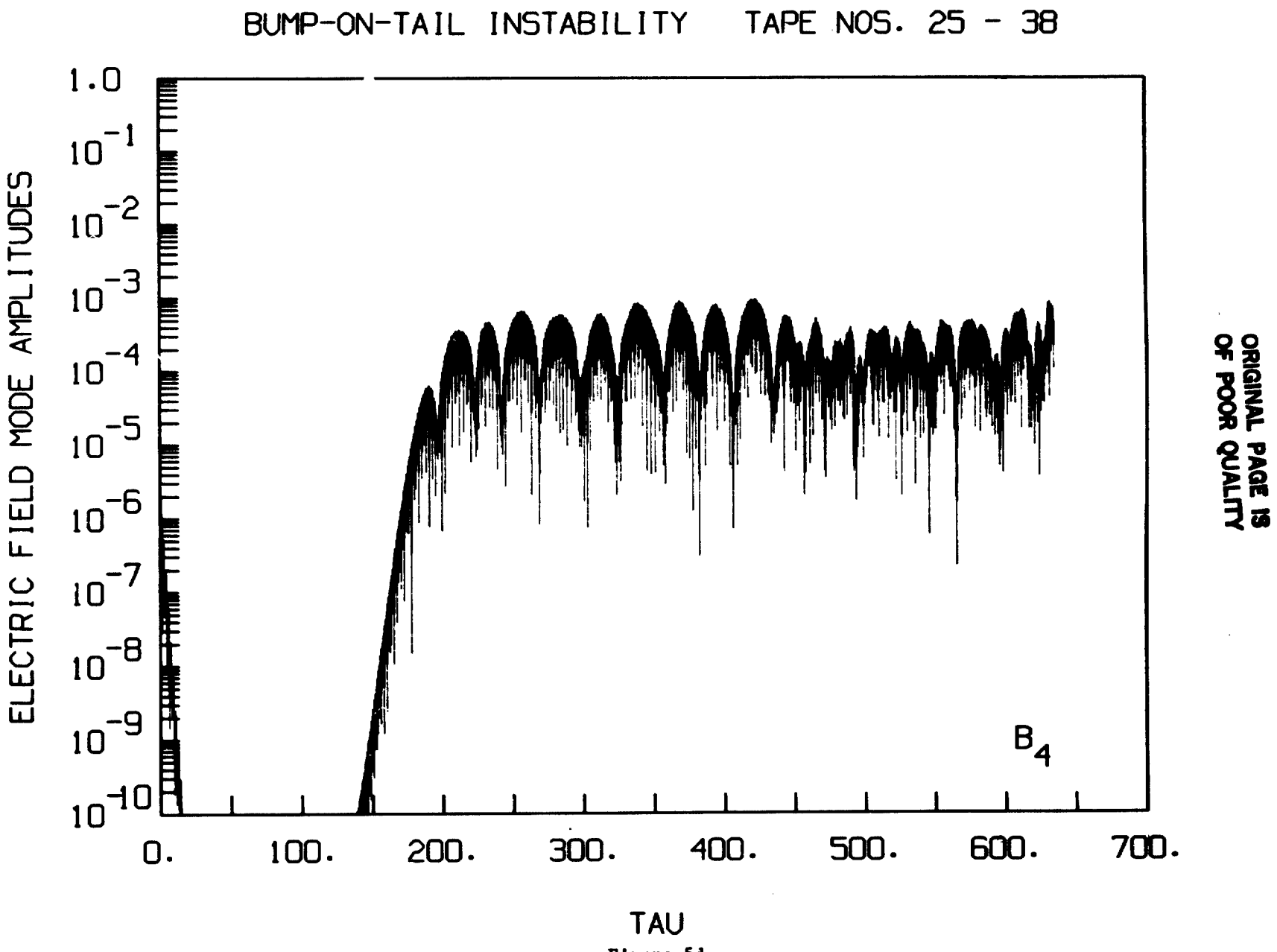

Figure 5d

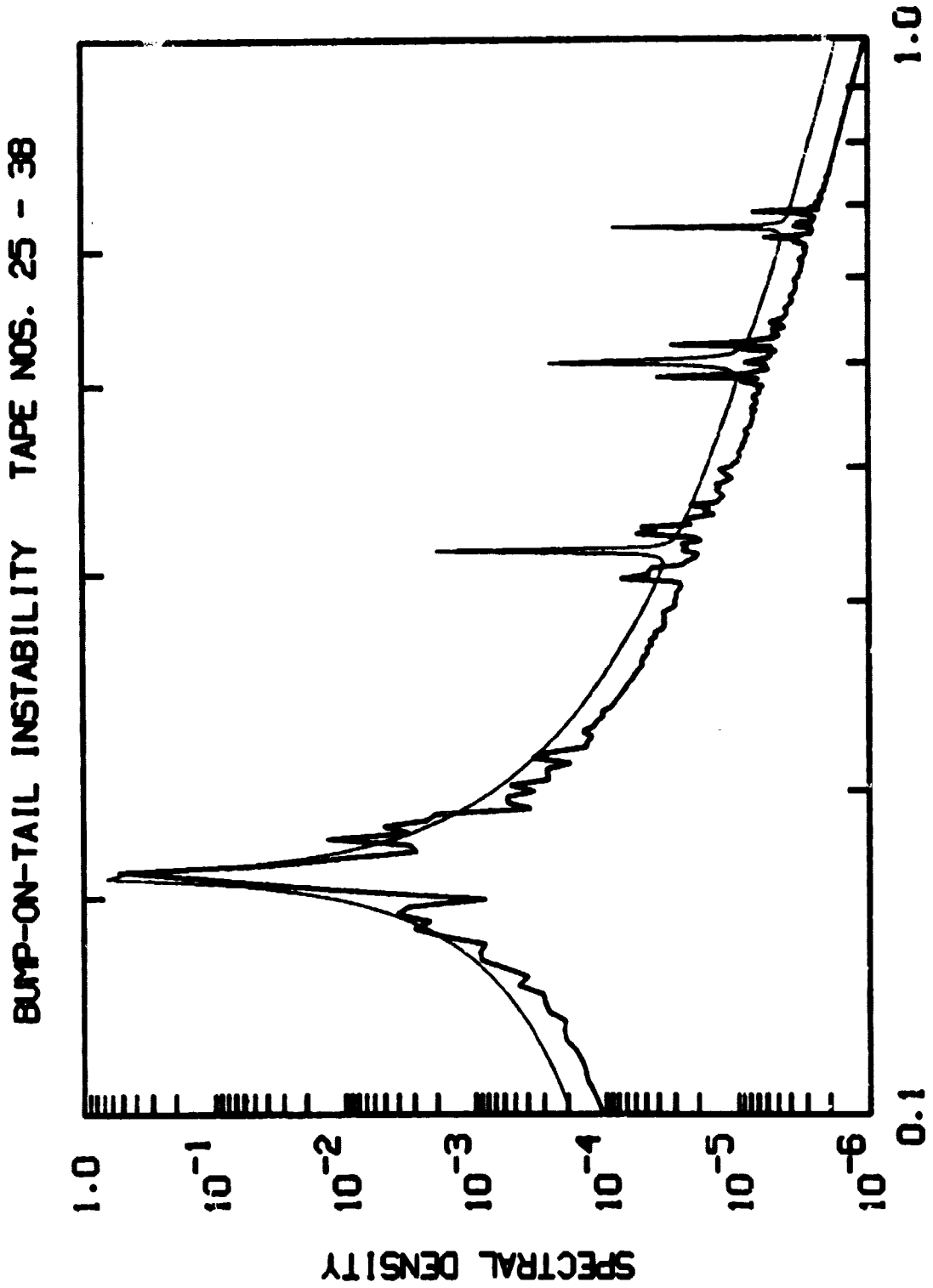

Figure 6

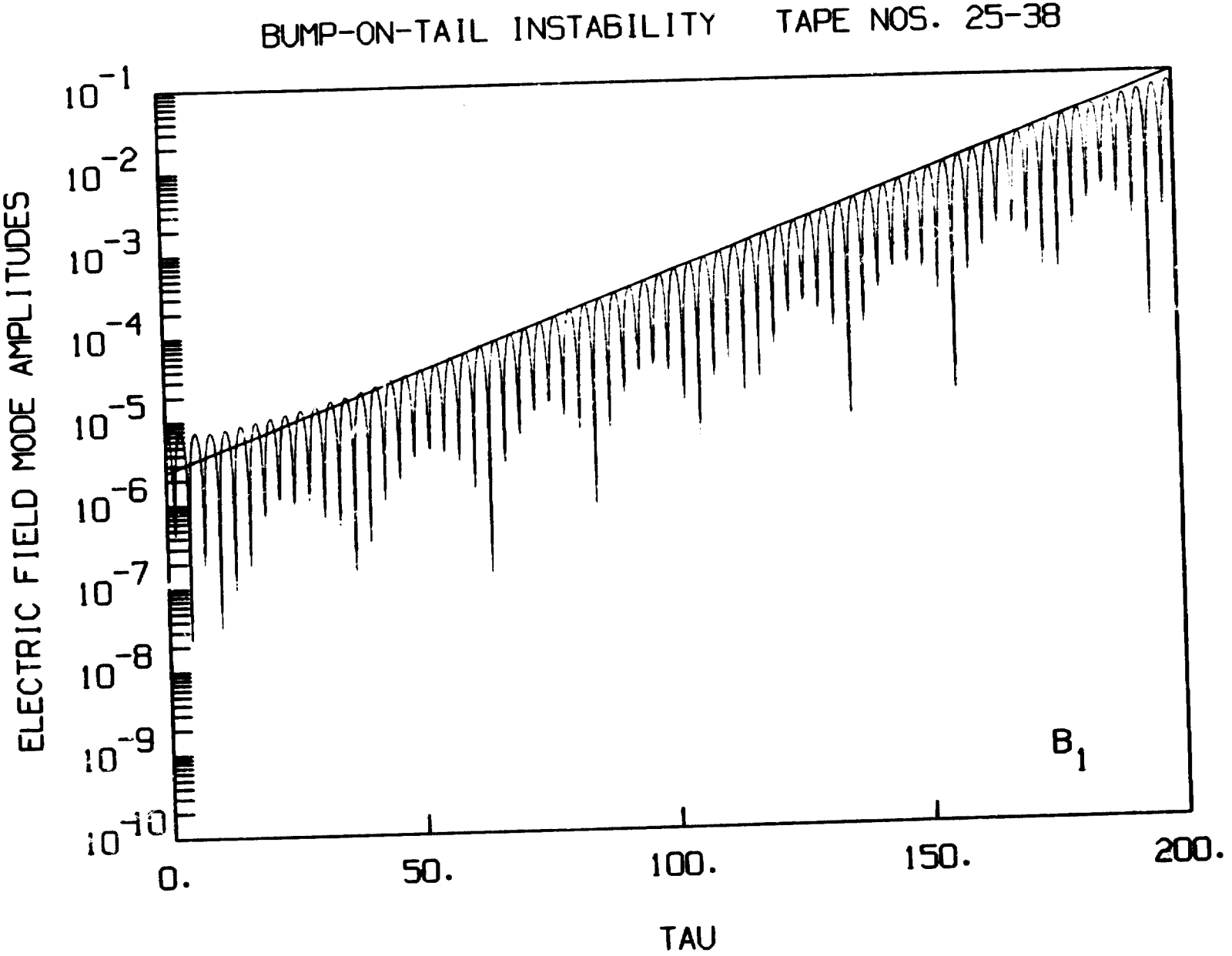

Figure 7

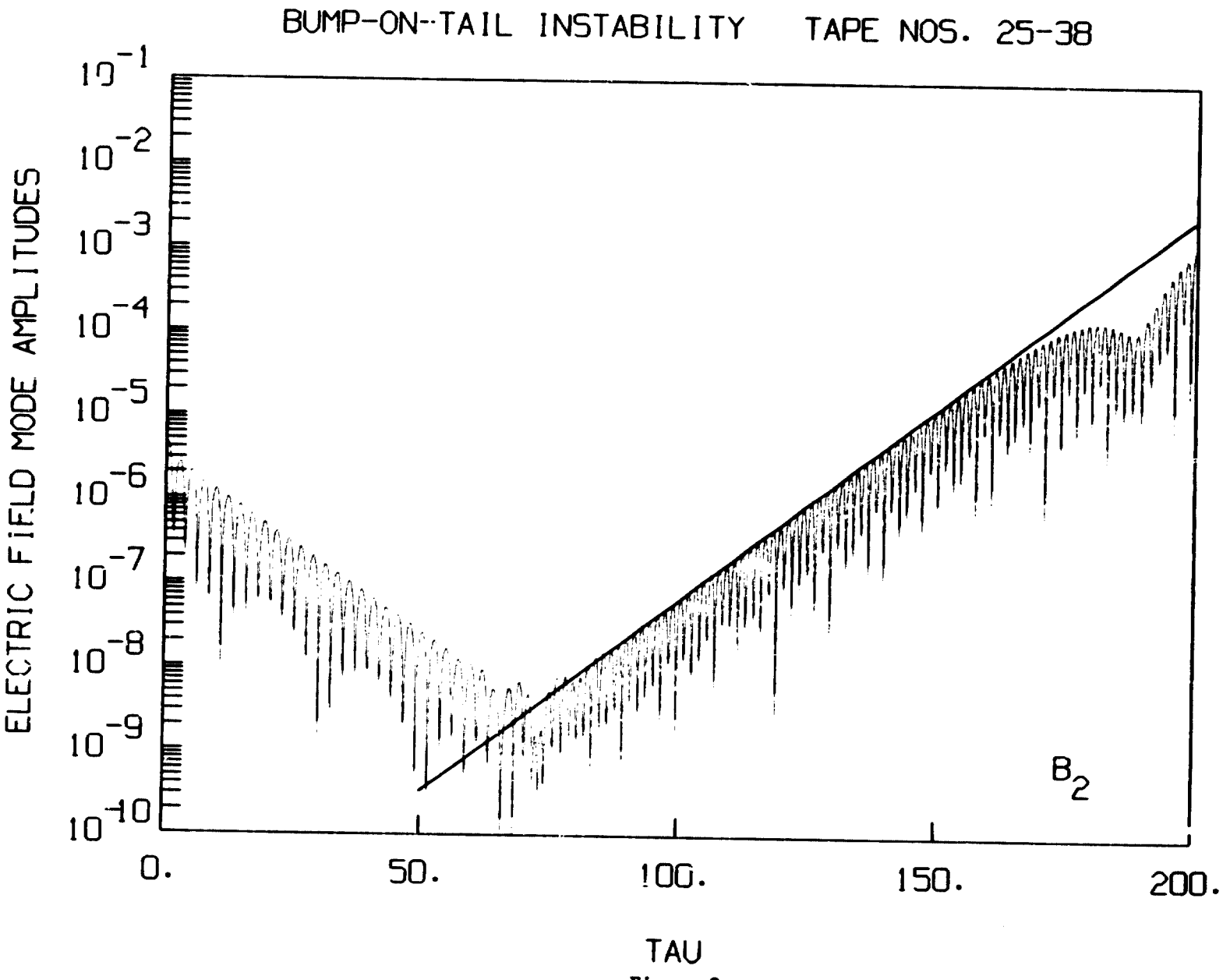

Figure 8